Methionine oxidation of Carbohydrate-Active enZymes during white-rot wood decay

Lise Molinelli, Elodie Drula, Jean-Charles Gaillard, David Navarro, Jean Armengaud, Jean-Guy Berrin, Thierry Tron, Lionel Tarrago

Methionine oxidation of Carbohydrate-Active enZymes during white-rot wood decay

Lise Molinelli[1,2], Elodie Drula[1,3], Jean-Charles Gaillard[4], David Navarro[1], Jean Armengaud[4], Jean-Guy Berrin[1], Thierry Tron[2], Lionel Tarrago[1,#]

From:

[1] Aix Marseille Univ., INRAE, Biodiversité et Biotechnologies Fongiques, Marseille, France

[2] Aix Marseille Univ., CNRS, Centrale Marseille, ISM2, Marseille, France

[3] Architecture et Fonction des Macromolécules Biologiques (AFMB), CNRS, Aix-Marseille Université, Marseille, France

[4] Université Paris-Saclay, CEA, INRAE, Département Médicaments et Technologies pour la Santé (DMTS), SPI, 30200 Bagnols-sur-Cèze, France

[#] To whom correspondence should be address: Lionel Tarrago (lionel.tarrago@inrae.fr)

Running title (51 characters): Met oxidation in CAZymes of white rot fungi during wood decay

Keywords: Carbohydrate-active enzymes, fungi, hydrogen peroxide, methionine oxidation, plant cell wall, redox proteomics, wood decay

Word count: 5037

Abstract

White-rot fungi employ secreted carbohydrate-active enzymes (CAZymes) along with reactive oxygen species (ROS), like hydrogen peroxide (H_2O_2), to degrade lignocellulose in wood. H_2O_2 serves as a co-substrate for key oxidoreductases during the initial decay phase. While the degradation of lignocellulose by CAZymes is well-documented, the impact of ROS on the oxidation of the secreted proteins remains unclear and the identity of the oxidized proteins is largely unknown. Methionine (Met) can be oxidized to Met sulfoxide (MetO) or Met sulfone ($MetO_2$) with potential deleterious, antioxidant, or regulatory effects. Other residues, like proline (Pro), can undergo carbonylation. Using the white-rot model *Pycnoporus cinnabarinus* grown on aspen wood, we analyzed the Met content of the secreted proteins and their susceptibility to oxidation combining labelled $H_2{}^{18}O_2$ with proteomics. Strikingly, their overall Met content was significantly lower (1.4%) compared to intracellular proteins (2.1%), a feature conserved in fungi but not in other eukaryotes. We also evidenced that a catalase, widespread in white-rot fungi, protects the secreted proteins from oxidation. Our redox proteomics approach allowed identification of 49 oxidizable Met and 40 oxidizable Pro residues within few secreted proteins, mostly CAZymes. Interestingly, many of them had several oxidized residues localized in hotspots. Some Met, including those in GH7 cellobiohydrolases, were oxidized up to 47%, with a substantial percentage of sulfone (13%). These Met are conserved in fungal homologs, suggesting important functional roles. Our findings reveal that white-rot fungi safeguard their secreted proteins by minimizing their Met content and by scavenging ROS and pinpoint redox-active residues in CAZymes.

Importance

The study of lignocellulose degradation by fungi is critical for understanding the ecological and industrial implications of wood decay. While carbohydrate-active enzymes (CAZymes) play a well-established role in lignocellulose degradation, the impact of hydrogen peroxide (H_2O_2) on secreted proteins remains unclear. This study aims at evaluating the effect of H_2O_2 on secreted proteins, focusing on the oxidation of methionine (Met). Using the model white-rot model *Pycnoporus cinnabarinus* grown on aspen wood, we showed that fungi protect their secreted proteins from oxidation by reducing their Met content and utilizing a secreted catalase to scavenge exogenous H_2O_2. The research identified key oxidizable Met within secreted CAZymes. Importantly, some Met like those of GH7 cellobiohydrolases, undergone substantial oxidation levels suggesting important roles in lignocellulose degradation. These findings highlight the adaptive mechanisms employed by white-rot fungi to safeguard their secreted proteins during wood decay and emphasize the importance of these processes in lignocellulose breakdown.

Introduction

Filamentous fungi are crucial in the carbon cycle because of their ability to decompose organic matter and release carbon back into the ecosystem (1). Wood-decay fungi extract carbon from recalcitrant polymers like cellulose and hemicelluloses embedded in a lignin matrix, by secreting enzymes into the extracellular environment (2). The secreted proteins, commonly referred to as the "secretome", contains the carbohydrate-active enzymes (CAZymes), including large sets of glycoside hydrolases (GH) and auxiliary activity (AA) enzymes (3, 4). The GH class contains the endo- and exo-acting enzymes targeting cellulose and hemicelluloses. The AA class contains laccases (AA1) and class II peroxidases (AA2) involved in lignin degradation, and lytic polysaccharide monooxygenases (LPMO, AA9) proposed to play an important role in the early phase of wood degradation (5–7). Reactive oxygen species (ROS), particularly hydrogen peroxide (H_2O_2), play a crucial role in the early phase of wood decay (8–10). H_2O_2 is generated by glucose-methanol-choline oxidoreductases (AA3) and copper radical oxidases (AA5), that target carbohydrate or aliphatic/aromatic alcohols (11, 12). In white-rot fungi, H_2O_2 acts as a co-substrate to fuels different types of LPMOs and AA2 peroxidases (13–15). While the roles of CAZymes and H_2O_2 during the degradation of lignocellulose is well-documented, the impact of ROS on the oxidation of CAZymes remains unclear. Fenton-generated ROS were shown to decrease enzymatic activity of some GHs in white-rot secretomes, through the oxidation of the secreted proteins, and the most abundant form of oxidation found was the oxidation of Met residues (16). Met can be converted by H_2O_2 into Met sulfoxide (MetO) or Met sulfone ($MetO_2$) and this has been shown to play critical roles in many organisms (17–20). For instance, Met oxidation can lead either to a loss of function or act as a regulatory switch, to activate enzymes (21, 22). The presence of oxidizable Met in proteins can also be associated to an antioxidant role by serving as a protection to avoid the oxidation of residues critical for the protein function (23). MetO can be reduced back to Met by the methionine sulfoxide reductases, but, as these enzymes are most likely not secreted they cannot reduce oxidized Met of secreted proteins (24). Regarding the importance of H_2O_2 during wood decay, our hypothesis is that some Met of secreted proteins can be oxidized and play antioxidant or regulatory

roles. Interestingly, the treatment of an α-galactosidase (GH27) from *Trichoderma reesei* with H_2O_2 strongly increased its activity due to the oxidation of a Met located near the active site, suggesting that Met oxidation of CAZymes can have a positive effect on their activity (25). To identify secreted proteins with oxidizable Met, we selected the white-rot *Pycnoporus cinnabarinus* grown on aspen wood as a model. *P. cinnabarinus* secretes H_2O_2-producing enzymes in the early phase of wood degradation, to provide co-substrate for the H_2O_2-consuming CAZymes (26), but also as potential oxidant of Met. We characterized the secreted proteins and investigated the sensitivity of their Met to oxidation by using a redox proteomics approach based on the use of ^{18}O-labeled hydrogen peroxide ($H_2{}^{18}O_2$) (27–30). Our investigations reveal the extend of Met oxidation in fungal secretomes and the precise localization of oxidizable residues in secreted proteins and CAZymes, suggesting potential antioxidant or regulatory roles.

Material and methods

Culture of P. cinnabarinus *on aspen wood.*

The dikaryotic strain *Pycnoporus cinnabarinus* CIRM-BRFM 145 was grown for 3, 5 or 7 days at as described (26). The media contained maltose (2.5 $g.l^{-1}$) and *Populus tremuloides* aspen sawdust particles of size < 2 mm (15 $g.\ l^{-1}$). Six replicates were mixed in pairs to obtain three replicate samples per time-point.

Preparation of P. cinnabarinus *secretomes and protein oxidation with* $H_2{}^{18}O_2$.

The culture supernatants containing the secreted proteins were centrifugated (1 h, 30,000xg, 10 °C) and sterilized by filtration (0.22 µm; Express Plus; Merck Millipore). The supernatants were equilibrated to pH 7 with 0.5 mM NaOH and the proteins were purified using two ion exchange chromatographies (**Fig. S1**): first, an anion exchange on DEAE Sephadex A-25 (Cytiva) and a cation exchange on CM Sephadex A-25 (Cytiva) for proteins not retained on the anion exchanger. Both resins were initially equilibrated with 20 mM sodium phosphate buffer (pH 7). Elution of the secreted proteins was performed with 1 M NaCl. Fractions from both anion and cation exchangers were pooled, desalted on Sephadex G-25 (PD-10 Desalting columns, Cytiva) in 50 mM sodium acetate (pH 5.2) and concentrated using Vivaspin polyethersulfone membrane (3 kDa cut-off, Sartorius). Protein concentrations were determined using the Bradford method (Bio-Rad) and the secretomes were used immediately. Secreted proteins (50 µg) were incubated 30 min with 1 mM hydroxylamine, desalted on Sephadex G-25 (PD SpinTrap, Cytiva), then incubated with 100 mM of $H_2{}^{18}O_2$ for 1 h in the dark, then desalted. Protein concentrations were determined, and the samples were stored at -20°C.

Proteomics analysis.

Proteins (15 µg) were precipitated trichloroacetic acid and processed for trypsin proteolysis as described (31). Peptides (5 µl) were injected into a nanoscale Easy-Spray™ PepMap™ Neo 2 µm C18 (75 µm x 750 mm) capillary column (Thermo Scientific) operated with a Vanquish Neo UHPLC system (Thermo Scientific) and resolved with a 65-min gradient of CH_3CN (5-40%), 0.1% formic acid, at a flow

rate of 0.25 µL per min. Data-dependent acquisition analysis of the peptides was performed with an Orbitrap Exploris 480 tandem mass spectrometer (Thermo) as described (32). Each full scan of peptide ions in the high-field Orbitrap analyzer was acquired from m/z 350 to 1800 at a resolution of 120,000, selecting only 2+ and 3+ charged precursors for high-energy collisional dissociation and with a dynamic exclusion of 10 seconds. MS/MS spectra of fragmented precursors were acquired at a resolution of 15,000 and assigned to peptide sequences by the MASCOT Server 2.5.1 search engine (Matrix Science) using the *P. cinnabarinus* annotated proteome, with fixed and variable modifications (**Datasets 3; 4**). Proteins were validated when at least two different peptides (p-value <0.01) were detected, resulting in a protein identification false discovery rate below 1%. Protein abundance was estimated using the Normalized Spectral Abundance Factor (NSAF) (33). The Met content of the proteins was calculated using the entire sequence. The Met content corrected by the NSAF was calculated using the following formula:

$$\frac{\sum(\%Met_{protein\ n}\ X\ NSAF_{protein\ n})}{\sum NSAF_{protein\ n}}$$

With $\%Met_{protein\ n}$ and $NSAF_{protein\ n}$ corresponding to the percentage of Met and the NSAF value of the individual proteins identified, respectively. The percentage of modification of Met or Pro residues was calculated by dividing the number of spectral counts (SC) of the residue with the modification by the total number of SC for the residue and then multiplying the result by 100. The mass spectrometry proteomics data have been deposited to the ProteomeXchange Consortium via the PRIDE (34) partner repository with the dataset identifier PXD046271 and 10.6019/PXD046271.

H_2O_2-consuming activity

Secreted proteins (20 µg) were incubated 1 h with H_2O_2 (30 mM) in sodium acetate buffer, pH 5.2. A control without proteins was done. Then, the samples were filtered using Vivaspin 3 kDa cut-off

and the remaining H_2O_2 in filtrates was titrated by absorbance measurement at 240 nm and compared to H_2O_2 concentration in controls.

Analysis of Met content in* P. cinnabarinus*, fungi, metazoans, and plants proteins.

P. cinnabarinus proteins were predicted secreted if they fulfilled three conditions: (i) presence of a secretion signal peptide, (ii) absence of endoplasmic reticulum retention motif and (iii) absence of transmembrane helix outside the signal peptide, as described (26). Experimentally validated fungal secreted proteins were retrieved from proteomics analyses (7, 35–49), from Uniprot (www.uniprot.org) and FunSecKB2 (50). Metazoans experimentally validated secreted were retrieved from Uniprot, MetazSecKB (51) and the Human Protein Atlas (52, 53). Experimentally validated plant secreted proteins were retrieved from Uniprot, PlantSecKB (54) and the SUBA database (55). The datasets of fungal, metazoans and plants non-secreted proteins were made using proteins retrieved from Uniprot, the Human Protein Atlas and the SUBA database. For all datasets, only manually curated proteins, and those found with least 5 SC in proteomics, were conserved. Membrane proteins, proteins shorter than 50 amino acids, or not starting with Met were discarded. Statistical analyses were unpaired t-test with Welch's correction.

Conservation of proteins and oxidized residues.

A hundred and twenty fungal genomes were selected based on their public availability and their representativity in the 9 fungal phyla (56, 57). Targets of the oxidized proteins were searched using BLASTP (v 2.6.0+) (58). The 100 sequences with the highest e-values were aligned using MAFFT tool (version 6.864b) (59). The conservation of individual residues was made by counting its occurrence in all the sequences.

Results

Optimized methods allowed to obtain secreted proteins representative of early days decay.

To identify oxidizable Met in the secreted proteins of *P. cinnabarinus*, we focused on the early days of wood decay, during which production and consumption of H_2O_2 are likely to occur (42). We performed a time-course growth of the fungus on aspen wood and purified the proteins from the culture supernatants at days 3, 5 and 7 on successive anion and cation exchange chromatography to avoid artifactual oxidation. Then, we oxidized the secreted proteins with $H_2{}^{18}O_2$ and identified them and their potential oxidative Met modifications using proteomics (**Fig. S1**). We identified 308 secreted proteins, among which CAZymes and proteases represented 41% and 10%, respectively (**Fig. 1; Table S1; Dataset 1**). Among the CAZymes, GH was by far the most represented class, with 89 proteins (71%) spread over 34 families (**Fig. 1; Table S1**). We identified most of the CAZymes expected during wood degradation, i.e. cellulases (GH3, GH5_5, GH5_9 and GH7, GH12, GH45), hemicellulases (GH10, GH43, GH51, CE15, CE16) (4), as well as pectinases (GH28, CE8) and also some CAZymes targeting fungal cell wall components (e.g. GH18 chitinases) (**Table S1**). Out of 23 identified AAs (18%), we found laccases (AA1) and class II peroxidases (AA2), LPMOs (AA9) and H_2O_2-generating enzymes (AA3, AA5). We estimated the abundance of the individual proteins using the Normalized Spectral Abundance Factor (NSAF) (**Dataset 1**). The mean %NSAF of all identified proteins was ~ 0.3% and 52 proteins were above this value. The most abundant protein categories were CAZymes (52%), proteins of unknown function (35%) and proteases (8%). Among the most abundant CAZymes, we found the three cellobiohydrolases (GH7), three chitinases (GH18) and two laccases (AA1). Interestingly, three H_2O_2-generating enzymes (two AA3_2 and one AA5_1) were among these most abundant CAZymes (**Dataset 1**). Overall, the identity of the secreted proteins and their abundance validated our approach, indicating that the growth conditions, the proteins preparation method, and the oxidative treatment used were suitable for studying Met sensitivity to oxidation.

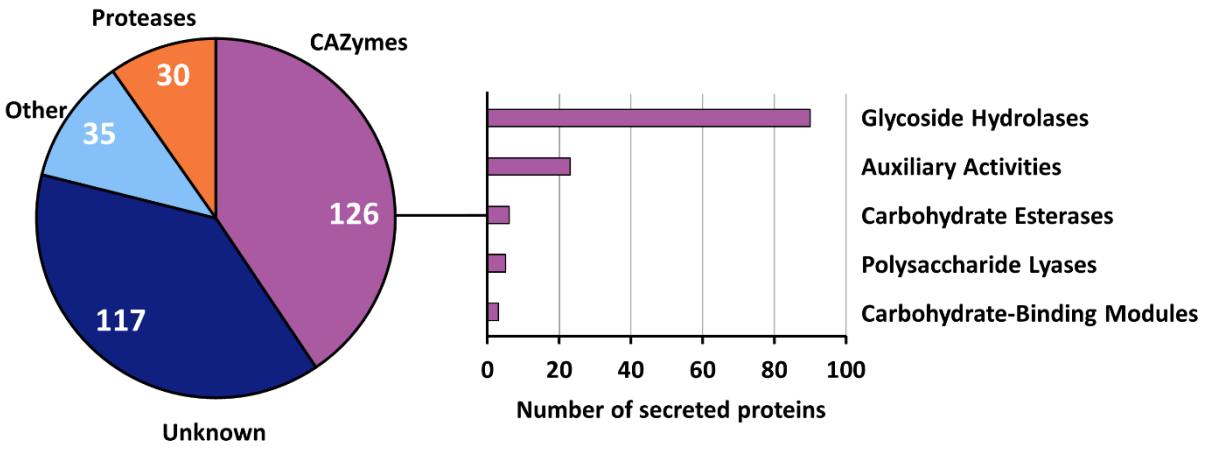

Figure 1. Distribution of the identified secreted proteins and CAZymes. Values shown are the aggregate of all replicates for each day (**Table S1; Dataset 1**). Bar graphs represent the number of CAZymes per class.

Met content is strongly reduced in fungal secreted proteins.

First, we evaluated the Met content of the secreted proteins, which was ~1.4% for each time-point (**Fig. 2A**). Then, to determine whether some abundant proteins with specific Met content could influence the overall content, we corrected the values by the proteins NSAF. The corrected Met contents were 1.21 ± 0.02, 1.33 ± 0.02, and 1.35 ± 0.02, for days 3, 5, and 7, respectively (**Fig. 2A**). These results indicate that the Met content in the proteins secreted by *P. cinnabarinus* is comprised between 1.2 to 1.4%. Strikingly, this value is twice lower than the Met content of proteins in general, i.e. 2.4% (60). We investigated whether this characteristic may apply to all secreted proteins of *P. cinnabarinus*. The theoretical *P. cinnabarinus* secretome consists of 666 proteins with an average Met content of 1.55 ± 0.82%, while the fungus non-secreted proteins have a higher mean of 2.07 ± 0.96% Met. (**Fig. 2B; Table S2; Dataset 2**). These results show that *P. cinnabarinus* secreted proteins contain significantly less Met than the non-secreted. Then, we compared the Met content of experimentally validated secreted proteins from fungi, metazoans, and plants with the Met content of intracellular proteins (**Fig. 2B; Table S2; Dataset 2**). Fungal secreted proteins have a mean Met content of 1.52 ± 0.74%, significantly lower than that of non-secreted proteins (2.17 ± 0.99%). In contrast, the Met content of metazoans secreted proteins (2.68 ± 1.40%) is significantly higher than that of the non-secreted proteins (2.41 ± 1.07%). No statistical difference exists between the Met content in secreted (2.59 ± 1.55%) and non-secreted (2.55 ± 1.14%) proteins of plants (**Fig. 2B; Table S2; Dataset 2**). Altogether, these results show that the secreted proteins of fungi contain less Met than the intracellular proteins, and that this feature is not conserved in other eukaryotes.

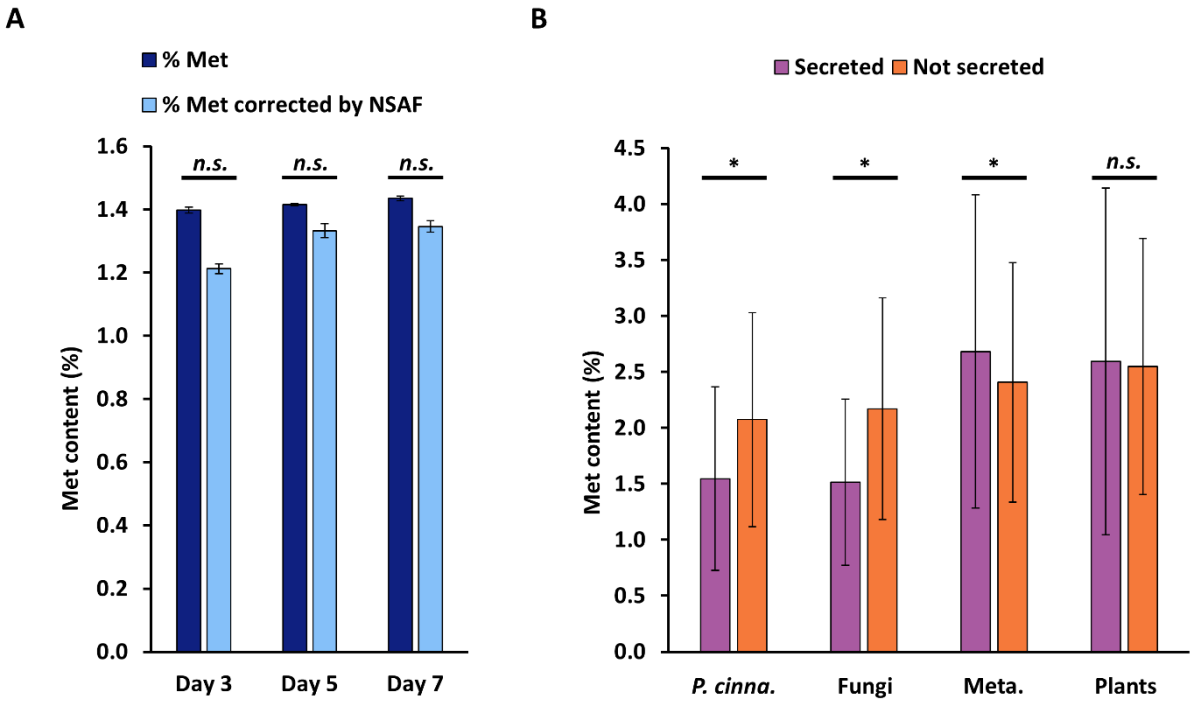

Figure 2. Met content of *P. cinnabarinus* secreted proteins and comparison with fungal, metazoan, and plant secreted and intracellular proteins. A) Met content of the identified *P. cinnabarinus* secreted proteins calculated for each protein and averaged for the three secretomes at each time point. Alternatively, the Met content for each protein was normalized by the protein NASF and averaged. Values shown are the mean of the 3 replicates ± SD. **B**) Met content of intracellular proteins and of secreted in the *P. cinnabarinus* theoretical proteome versus the Met content of experimentally validated intracellular and secreted proteins from fungi, metazoans, and plants (**Table S2; Dataset 2**). Values shown are the mean of all proteins in each set ± SD. Statistical analysis performed by unpaired t-test with Welch's correction (*$P \leq 0.001$; *n.s.*, not significant).

A catalase protects secreted proteins from oxidation.

The identification of oxidizable Met in *P. cinnabarinus* secreted proteins required accurate quantification of their oxidation levels. $H_2{}^{18}O_2$ was used to prevent artifactual Met oxidation potentially occurring during sample preparation by blocking the Met reduced in the samples and converting them to Met sulfoxide or sulfone containing ^{18}O atom (Met^{18}O and Met$^{18}O_2$, respectively). The use of a concentrated $H_2{}^{18}O_2$ solution (100 mM) should allow the oxidation of all the reduced Met and the reliable quantification of the initial levels of Met^{16}O and Met$^{16}O_2$ (28, 29). For the day 3 secretome, the levels of Met carrying ^{18}O or ^{16}O, either as sulfoxide or sulfone, were ∼64% and ∼18%, respectively. Although, ∼18% of Met in reduced form were still present, this indicated that most Met from the identified proteins were oxidized after the treatment with $H_2{}^{18}O_2$. Of note, ^{16}O or ^{18}O sulfone levels reached ∼2% (**Fig. 3A; Table S3; Dataset 3**). On the contrary, in day 5 and day 7 secretomes, the levels of MetO and MetO_2 carrying ^{18}O were extremely low (∼1%), indicating that the blocking strategy failed for these samples (**Fig. 3A; Table S3; Dataset 3**). To evaluate whether this lack of oxidation by $H_2{}^{18}O_2$ in secretomes of days 5 and 7 affected only Met residues, we reanalyzed our data by searching for two main forms of Pro carbonylation bearing ^{18}O. For the day 3 secretome, we found slightly less than 4% of Pro oxidized with ^{18}O. A similar content of ^{16}O was found, indicating that the large majority of Pro were not oxidized (∼92%) (**Fig. 2B; Table S4; Dataset 4**). This low level of Pro oxidation was anticipated due to its low reactivity with $H_2{}^{18}O_2$ (61). The percentage of ^{18}O oxidation decreased to ∼0.5% in the day 5 and day 7 secretomes, while ^{16}O oxidation levels remained comparable to those observed for the day 3 secretome. Thus, the trend for Pro is the same as for Met indicating that the lack of oxidation observed for Met was not specific to this residue. Proteins secreted during the days 5 and 7 of decay were not oxidized by exogenous $H_2{}^{18}O_2$, unlike those secreted at day 3. These results prompted us to search for secreted enzymes that scavenge H_2O_2. A catalase stood out: almost absent at day 3 (0.02 ± 0.02 %NSAF), but more abundant at days 5 and 7, with %NSAF values of 0.33 ± 0.05 and 0.42 ± 0.01, respectively (**Fig. 2C; Dataset 1**). When we measured the H_2O_2-consumming activity of the secretomes, we observed no activity at day 3, but strong activities at days 5 and 7 secretomes, in a perfect

consistency with the catalase abundance (**Fig. 2C**). Although few potential peroxidases and LPMOs were present, there was no difference in their abundance during the time course (**Dataset 1**). These results indicated that this catalase was very likely responsible for most, if not all, of the H_2O_2-consuming activity. Altogether, these results show that, under our experimental conditions, *P. cinnabarinus* secreted a catalase at days 5 and 7, which, by consuming potential exogenous H_2O_2, protected the secreted proteins from oxidation. On the contrary, at day 3, the secreted proteins are left without any protection against exogenous oxidant. On the other hand, this highlight that the strategy consisting of using high concentrations of $H_2{}^{18}O_2$ to block reduced Met can hardly be applied to the secretomes collected at days 5 and 7, at least in conditions where hydroxylamine was not an efficient inhibitor of H_2O_2-consuming activity. Nonetheless, since Met oxidized with ^{18}O were detected, we analyzed the nature of the oxidized proteins to identify Met residues with potential antioxidant or regulatory roles.

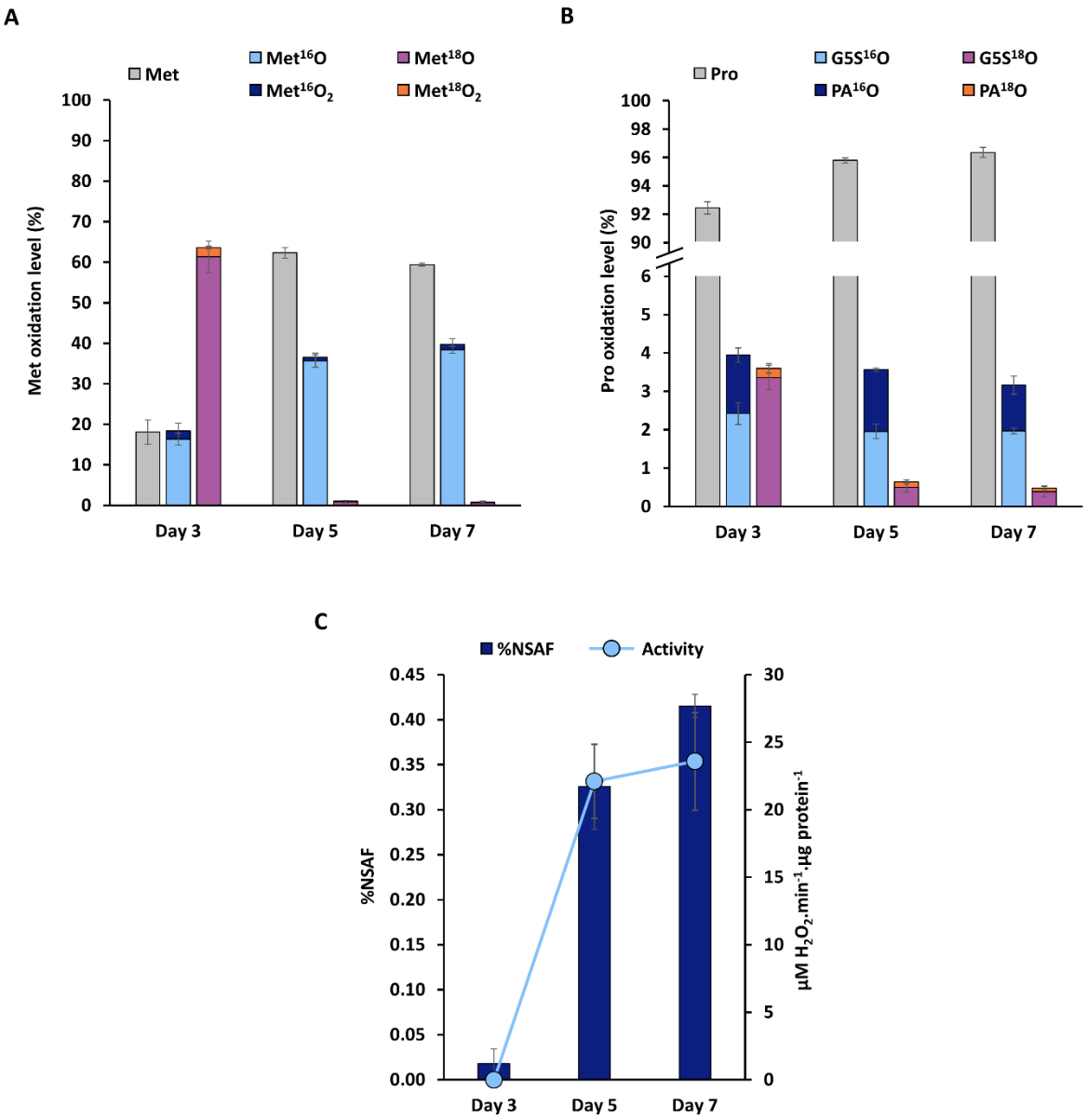

Figure 3. Levels of Met and Pro oxidation in the *P. cinnabarinus* secretomes and H_2O_2-consuming activity. A) Total levels of Met oxidation as sulfoxide and sulfone, either ^{16}O or ^{18}O calculated using the spectral counts of all Met-containing peptides and compared to the level of non-oxidized Met for each time point (**Table S3; Dataset 3**). **B)** Total levels of Pro oxidation as glutamic 5-semialdehyde (G5S) and pyroglutamic acid (PA), either ^{16}O or ^{18}O calculated using the spectral counts of all Pro-containing peptides and compared to the level of non-oxidized Pro for each day (**Table S4; Dataset 4**). **C)** %NSAF of the catalase A0A060STN2 (**Dataset 2**) and total H_2O_2-consuming activity at each time point.

Most of the oxidations occur on a few secreted CAZymes.

Among the 308 secreted proteins identified, we detected 265 Met belonging to 118 proteins (**Table S3; Dataset 3**). We selected only the Met-containing peptides present in all replicates for each secretome, with at least five spectral counts, in at least two out of the three replicates. At day 3, all selected Met were found oxidized with ^{18}O (**Fig. 4A; Dataset 3**). The total oxidation (^{16}O and ^{18}O) ranged from ~ 20% to 100% for the 46 identified Met (**Fig. 4A**). Four Met, all from CAZymes, were fully oxidized and thus saturated with ^{18}O: Met305 of a PL35, Met378 of a GH7, Met314 of a PL8, and Met239 of a CE16 (**Fig. 4A; Dataset 3**). Twenty-four proteins had oxidation levels ranging from ~81% to 97% and 17 from 57% to ~80%. Only the Met592 from an AA3_2 displayed a much lower value of total oxidation (~20%) (**Fig. 4A; Dataset 3**). The quantification of the ^{16}O-oxidation levels appeared clear for the four ^{18}O-saturated Met and should correspond to the levels "naturally" found during the wood decay. However, for all other Met with an oxidation value less than 100%, the saturation with ^{18}O was incomplete and some artifactual oxidation may have occurred during the sample preparation, and thus the level of ^{16}O might be overestimated. For these proteins, we assumed that the percentage of ^{16}O found during wood decay was necessarily equal to or lower than the measured one. The percentage of oxidation as ^{16}O ranged from 0% to 47% with a mean of 18% (**Fig. 4A; Dataset 3**). This value is consistent with the mean percentage of Met^{16}O oxidation calculated considering all Met containing-peptides found (**see Fig. 3A**) and indicated that most of the oxidation was concentrated on these few secreted proteins. Concerning day 5 and day 7 secretomes, the very low levels of ^{18}O oxidation precluded the use of the blocking strategy. However, to find proteins with Met^{18}O may allow to consider $H_2{}^{18}O_2$ as a probe for highly reactive residues, because of the low $H_2{}^{18}O_2$ concentration they were exposed to, due to the catalase activity. We found eight and nine Met bearing ^{18}O in the proteins secreted at day 5 and day 7, respectively, and five were common to both samples (**Fig. 4B; Dataset 3**). The percentages of ^{18}O ranged from ~2% to ~14%, and from ~1% to ~23%, for the secreted proteins of day 5 and day 7, respectively. Among the 11 oxidized Met, only three were uniquely found at day 5 or day 7: Met533 of a GH95 at day 5, and Met284 and Met160 belonging to a PL35 and a GH3,

301 respectively, at day 7 (**Fig. 4B; Dataset 3**). This indicates that most of the proteins found oxidized with
302 ^{18}O at day 5 or 7 were also oxidized at day 3, highlighting their high reactivity to H_2O_2. We found a total
303 number of 49 oxidizable Met belonging to 28 proteins, representing ∼24% and ∼19% of all the
304 identified Met and proteins from the secretome, respectively (**Fig. 4C; Dataset 3**). Interestingly, the 18
305 identified CAZymes represented most of them (64%), while proteases and proteins of unknown
306 function both represented 18% with five identified proteins. The most represented CAZymes were GHs
307 with 10 identified proteins. These results indicates that the proportion of oxidized CAZymes was
308 enriched compared to the different types of proteins present in the secretomes (**compare Fig. 4C with**
309 **Fig. 1**).

310

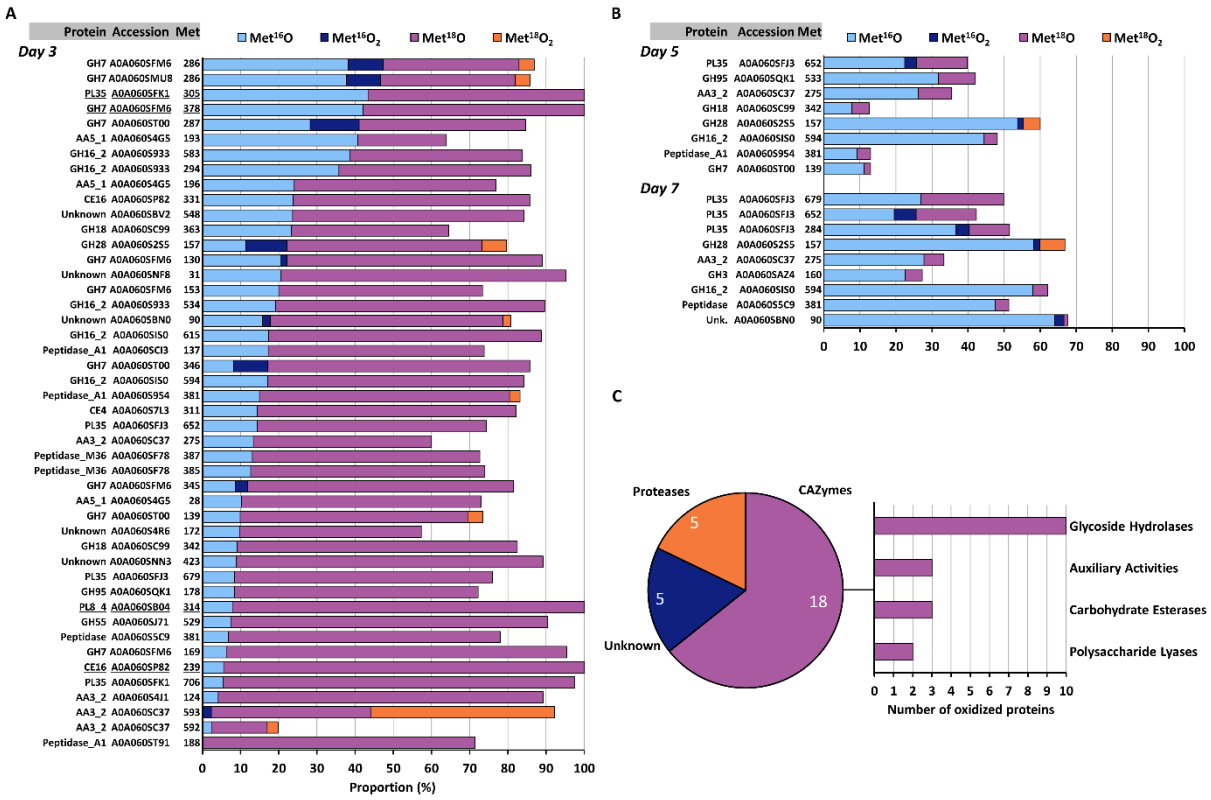

Figure 4. Identity of oxidized Met and their levels of oxidation in *P. cinnabarinus* secretomes. A) Proportion of the different forms of oxidation for the Met identified in the secreted proteins at day 3. Proteins are ranked based on the percentage of ^{16}O (MetO and $MetO_2$). The four Met fully oxidized are underlined. Values shown are the mean of oxidation without standard deviation, omitted for clarity. All values are in **Dataset 3**. **B)** Proportion of the different forms of oxidation for the Met identified in the secreted proteins at day 5 and day 7. Proteins are ranked based on the percentage of ^{18}O (MetO and $MetO_2$). All values are in **Dataset 3**. **C)** Distribution of the identified secreted proteins and CAZymes with oxidized Met. Values shown are the aggregate of all replicates for each time point (**Dataset 3**). Bar graphs represent the number of CAZymes per class.

Oxidation occurs in multiple sites and hotspots of homologous proteins.

Interestingly, among the five most oxidized, three Met belong to the three GH7 (A0A060SFM6, A0A060SMU8, A0A060ST00, named A, B, and C, respectively), at position 286 of the GH7 A and B, and at position 287 of the GH7 C (**Fig. 4A**). A sequence alignment showed that these positions are conserved between these GH7 homologs (**Fig. 5A**). These Met were oxidized with similar levels of $Met^{16}O$ (between 28% and 38%) and $Met^{16}O_2$ (between 9% and 13%). We also detected seven other oxidized Met on these GH7s, four were uniquely on the GH7 A, one on the GH7 B, and two were in a position conserved in GH7 A and B. Since we had assessed the overall level of Pro oxidation, we quantified the percentage of oxidation of individual Pro, considering only those labeled with ^{18}O (**Dataset 4**). GH7 A had four oxidized Pro, two of which were in positions conserved into the GH7 B (**Fig. 5A**). Interestingly, we found that oxidation of Met and/or Pro occurred on homologs of GH16_2, PL35, proteases and GH152 (**Fig. 4; Fig. S2**). This represented 11 proteins among the 33 proteins identified having oxidized residues (28 with Met with or without Pro and 5 with Pro only) (**Fig. 4; Fig. S2; Datasets 3; 4**). Moreover, 19 out of the 33 identified proteins were oxidized on multiple residues, from two to 10. A GH152 was oxidized on 8 Pro, while the GH7 A was the protein with the highest number of oxidation sites (10), including six Met and four Pro (**Fig. 4; Fig. 5; Fig. S2; Datasets 3; 4**). Finally, several oxidation sites were located close to each other in the protein sequences, forming "hotspots" like the Pro343 and Met345, and three other Pro of the GH7 A (**Fig. 5A**). In total, we counted 24 occurrences of sites containing two oxidized residues in the protein sequences (**Fig. 5B**). Analysis of a tridimensional model of GH7 A revealed that oxidized residues distant on the sequence may be close on the structure, as the Met130 and Met160, the Met153 in the vicinity of three Pro, and the Met286 clustered with the Pro343 and Met345 (**Fig. 5C**). Altogether, these results indicate that most of the oxidation affects a relatively small set of CAZymes that can be oxidized at multiple positions, with some hotspots. Moreover, the fact that oxidized residues were found at similar positions within the homologs of *P. cinnabarinus* secreted proteins suggests that these residues have been conserved to fulfill antioxidant or regulatory roles.

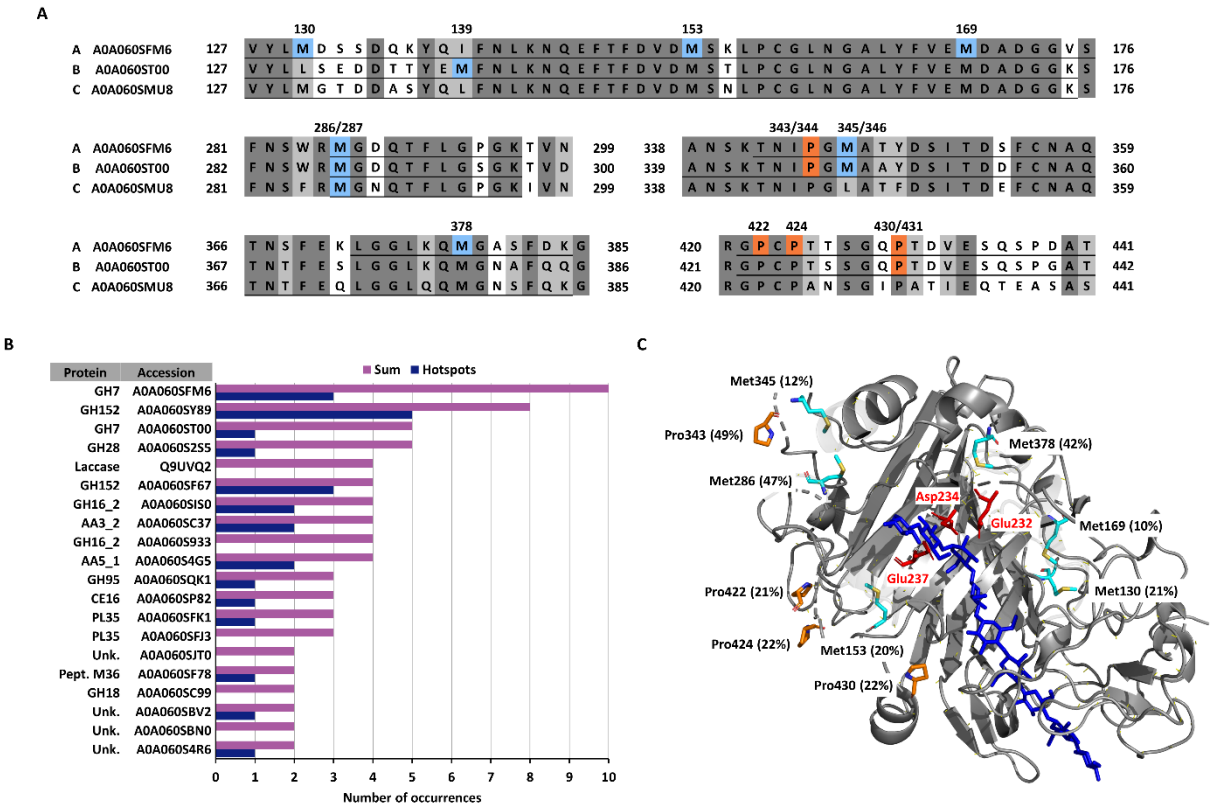

Figure 5. Partial sequence alignment of GH7, numbers of oxidation sites and hotspots in identified secreted proteins and tridimensional model of GH7. A) Oxidized Met and Pro residues are on *blue* and *orange* background, respectively. *Dark* and *light grey* backgrounds represent strictly conserved and similar amino acids, respectively. Position and percentage of oxidation of the residues are indicated above the sequence. For Pro, the percentage presented correspond to the sum of all oxidized forms, either ^{16}O or ^{18}O at day 3, excepted the one indicated with 'D5', corresponding to Pro oxidation at day 5. Underlined sequences represent peptides detected by LC-MS/MS. Accession numbers are on the left of the sequences. **B**) Values correspond to the total number of oxidizable Met and Pro sites found per protein. Hotspots correspond to the number of times that two oxidizable sites were located within a window of ten amino acids on the protein sequence. All data are presented in **Datasets 3 and 4**. **C**) 3D model of the GH7 A0A060SFM6 downloaded from Alphafold database (62). The position of the cellonoanose substrate (in *blue*) was modelized using the experimentally determined structure of *Trichoderma reesei* Cel7A (PDB #4C4C). Met and Pro found oxidized are represented as *cyan* and *orange* sticks, respectively. Catalytic residues are represented as *red* sticks. Percentage of oxidation at day 3 are in brackets. Some parts of the protein were rendered transparent for clarity.

Conservation suggests a list of residues with antioxidant or regulatory roles.

To determine whether oxidized residues found in *P. cinnabarinus* proteins were widely conserved, we searched for homologs of the 33 proteins having oxidized residues in homologs from other fungi and quantified the conservation of the 89 oxidized residues. Our hypothesis was that oxidizable residues playing antioxidant or regulatory roles are more likely to be conserved among distantly related organisms, as shown for Met of actin or of the ffh/SRP proteins (63–65). To avoid overrepresentation of sequences coming from closely related organisms, the search was made in 120 representative fungal species, covering the nine fungal phyla (**Dataset 5**). Overall, the conservation of Met or Pro ranged from 1% to 100%, with a mean of 49%. Considering only residues with conservation values above 75%, and found in more than 80 sequences, we obtained a list of nine Met and nine Pro at conserved positions in 14 secreted proteins (**Table 1**). The GH7 A has four conserved Met, among which Met 169 conserved in 99% of the homologs, and a conserved Pro. Other Met are conserved in the GH7 B and C, and in two GH16_2, one GH18, one AA3_2 and a peptidase M36, present in all fungi (**Table 1; Dataset 5**). Regarding Pro, three are conserved in all homologs, at positions 614, 143 and 441 of a GH16_2, a GH28 and a laccase, respectively. Conserved Pro were also found in a AA3_2, an unknown protein and a GH152 (**Table 1; Dataset 5**). These results allowed identification of proteins with oxidizable Met and Pro residues strongly conserved across the fungal phyla.

Table 1. *P. cinnabarinus* secreted proteins with oxidized residues conserved across fungal proteins. Only proteins for which the number of identified homolog sequences identified was higher than 80 were considered. The complete list of identified secreted proteins is presented in **Dataset 5**.

Accession Uniprot (JGI)	*Description*	*Repartition (Nb. of sequences)*	*Residue*	*Conservation (%)*
A0A060SFM6 (8640)	GH7	Dikarya (98)	Met 130	80
			Met 169	99
			Met 286[a]	76
			Met 378	83
			Pro 430[b]	99
A0A060ST00 (6809)	GH7	Dikarya (98)	Met 287[a]	76
			Pro 431[b]	99
A0A060SMU8 (5845)	GH7	Dikarya (98)	Met 286[a]	76
A0A060SIS0 (301)	GH16_2	Basidiomycota (100)	Met 615	92
			Pro 614	100
A0A060S933 (3097)	GH16_2	Basidiomycota (91)	Met 583	83
A0A060SC99 (6004)	GH18	Dikarya, Mucor., Zoo. (99)	Met 342	86
A0A060S4J1 (1984)	AA3_2	Agaricomycetes (100)	Met 124	83
A0A060SF78 (8374)	Pep. M36	All fungi (100)	Met 387	81
A0A060S2S5 (8001)	GH28	Dikarya (99)	Pro 143	100
Q9UVQ2 (8672)	Laccase	Basidiomycota (100)	Pro 284	96
			Pro 441	100
A0A060SC37 (3147)	AA3_2	Dikarya (98)	Pro 594	97
A0A060S4R6 (3419)	Unknown	Dikarya, Mucor., Chytridio., Neo. (100)	Pro 170	83
A0A060SF67 (3180)	GH152	Dikarya, Mucoromycota (99)	Pro 184[c]	94
A0A060SY89 (5455)	GH152	Dikarya, Mucor., Chytridio. (99)	Pro 200[c]	96

[a, b, c] Conserved positions between the *P. cinnabarinus* homologs. *Mucor., Mucoromycota; Zoo., Zoopagomycota, Chytridio., Chytridiomycota, Neo., Neocallimastigomycota.*

Discussion

Taking a white-rot wood decayer as model, we showed that fungal secreted proteins have a strongly reduced Met content (~1.4%) compared to the non-secreted (~2.1%) and that this feature is not conserved in metazoans and plants. This decreased Met content suggests that protection of proteins secreted by fungi is achieved by avoiding oxidation, in line with the previously proposed mechanism (16). Interestingly, these data contrast with those obtained from animal studies which showed that proteins encoded by the mitochondrial genome may contain up to 6-10% Met. This high content could act as an endogenous antioxidant with the exposed Met scavenging ROS which are then removed by methionine sulfoxide reductases in a cycle of oxidation and reduction (66). A similar mechanism was proposed in bacteria (67, 68). The absence of external system of MetO reduction preclude the use of such mechanism with fungal secreted proteins (24). This protection is most likely accompanied by the secreted catalase we found (**Fig. 3**), in line with previous assumptions (16, 69–71). The secretion of a catalase by *P. cinnabarinus* was unexpected, as it has not been previously detected (41, 42), nor has extracellular activity been measured for the white-rot *Phanerochaete chrysosporium* (72). However, searching for secreted catalase homologs, we found that it is widespread in basidiomycota, and particularly in white-rot fungi (**Table S5**), contrary to previous phylogenetic analysis (73). Lack of detection of the protein or its activity may be due to specific expression conditions. In white-rot, it is surprising that a catalase was expressed along with H_2O_2 producing and consuming enzymes. However, catalases have Km values in the mM range (70), and their action could result in lowering the H_2O_2 concentration below a levels that is damaging to proteins, but allows the activity of H_2O_2-driven oxidoreductases.

Using $H_2{}^{18}O_2$-based proteomics, we identified oxidizable Met and highlighted that CAZymes were the most oxidized secreted proteins during wood-decay, and that Met oxidation could occur on several residues, sometimes clustered in hotspots. Clustering was also observed in bacterial proteins (74), suggesting a universal phenomenon. The blocking strategy we used is based on a saturation of

reduced Met with ^{18}O. However, saturation was difficult to achieve, with only 4 Met saturated with ^{18}O in the day 3 secretome (**Fig. 4**). An initial denaturation step would have probably allowed $H_2{}^{18}O_2$ to access the Met buried in the protein core (28). However, as our goal was to identify secreted proteins with potential oxidizable Met we chose not to denature them. Our idea was that an oxidizable Met should be accessible to an oxidant, either natural or $H_2{}^{18}O_2$. The results at day 3 argue for the accessibility of the Met to $H_2{}^{18}O_2$, as the percentage of ^{18}O was higher than that of ^{16}O for 43 Met out of 46. As artifactual ^{16}O-oxidation cannot be ruled out, the percentage of ^{16}O was necessarily lower or equal to those measured. In our study, the mean percentage of ^{16}O was 18%, while in studies on animals using similar approaches, it was ~4% (27, 28), arguing for potential artifactual oxidation. However, while intracellular proteins are protected by methionine sulfoxide reductases and ROS scavengers, the MetO in secreted proteins cannot be reduced, and no H_2O_2-consuming was detected in the secretome at day 3. Thus, to find high levels of MetO in fungal secreted proteins is expected. Interestingly, nine Met were oxidized as ^{16}O sulfone among which five were also oxidized as $Met^{18}O_2$ (**Fig. 4**), confirming their propensity to form sulfone during wood decomposition.

Some of the Met we found oxidized in *P. cinnabarinus* are conserved throughout the fungal kingdom, suggesting potentially important roles (**Table 5**). They could act as antioxidants, as for the GH7 whose Met and Pro are located at the surface of the proteins and in the substrate cleft (**Fig. 5C**), potentially preventing critical residues from being oxidized, as proposed for a glutamine synthetase (23). Oxidizable Met could also have a functional role altering enzyme activity, like for a GH18 in which a conserved oxidized Met is located near the catalytic residue (**Fig. S3**), as shown for a GH27 galactosidase of *T. reesei* (25). In conclusion, our findings highlight a common mechanism in fungi preventing oxidation of secreted proteins and, pinpoint redox-regulated CAZymes to be further characterized.

Acknowledgments

The authors kindly thank the CIRM-CF for providing the *P cinnabarinus* CIRM-BRFM145 strain, Dan Cullen (Forest Product Laboratory, USDA, Madison, WI, USA) for providing *Populus tremuloides* wood, and Marie-Noëlle Rosso (Aix Marseille Univ., INRAE, Biodiversité et Biotechnologies Fongiques) for critical reading of the manuscript. This work received support from the French government under the France 2030 investment plan, as part of the Initiative d'Excellence d'Aix-Marseille Université —IM2B (AMX-19-IET-006) for L.M. and L.T. – A*MIDEX (AMX-21-PEP-028) for L.T. The authors would like to thank the NovoNordisk foundation (OxyMiST project, grant number NNF20OC0059697).

CRediT author statement

Lise Molinelli: Conceptualization, Methodology, Validation, Formal analysis, Investigation, Data Curation, Writing - Original Draft, Writing - Review & Editing, Visualization, **Elodie Drula:** Software, Methodology, Formal analysis, Investigation, Data Curation, **Jean-Charles Gaillard:** Formal analysis, Investigation, **David Navarro:** Investigation, Resources, **Jean Armengaud:** Formal analysis, Resources, Data Curation, Writing - Review & Editing, **Jean-Guy Berrin:** Resources, Writing - Review & Editing, Funding acquisition, **Thierry Tron:** Conceptualization, Resources, Writing - Review & Editing, Supervision, Funding acquisition, **Lionel Tarrago:** Conceptualization, Methodology, Software, Validation, Formal analysis, Investigation, Resources, Data Curation, Writing - Original Draft, Writing - Review & Editing, Visualization, Supervision, Funding acquisition.

References

1. Fabian J, Zlatanovic S, Mutz M, Premke K. 2017. Fungal–bacterial dynamics and their contribution to terrigenous carbon turnover in relation to organic matter quality. ISME J 11:415–425.

2. Baldrian P, Valášková V. 2008. Degradation of cellulose by basidiomycetous fungi. FEMS Microbiol Rev 32:501–521.

3. Drula E, Garron M-L, Dogan S, Lombard V, Henrissat B, Terrapon N. 2022. The carbohydrate-active enzyme database: functions and literature. Nucleic Acids Res 50:D571–D577.

4. Hage H, Rosso M-N. 2021. Evolution of Fungal Carbohydrate-Active Enzyme Portfolios and Adaptation to Plant Cell-Wall Polymers. 3. J Fungi 7:185.

5. Couturier M, Ladevèze S, Sulzenbacher G, Ciano L, Fanuel M, Moreau C, Villares A, Cathala B, Chaspoul F, Frandsen KE, Labourel A, Herpoël-Gimbert I, Grisel S, Haon M, Lenfant N, Rogniaux H, Ropartz D, Davies GJ, Rosso M-N, Walton PH, Henrissat B, Berrin J-G. 2018. Lytic xylan oxidases from wood-decay fungi unlock biomass degradation. Nat Chem Biol 14:306–310.

6. Harris P V., Welner D, McFarland KC, Re E, Navarro Poulsen J-C, Brown K, Salbo R, Ding H, Vlasenko E, Merino S, Xu F, Cherry J, Larsen S, Lo Leggio L. 2010. Stimulation of Lignocellulosic Biomass Hydrolysis by Proteins of Glycoside Hydrolase Family 61: Structure and Function of a Large, Enigmatic Family. Biochemistry 49:3305–3316.

7. Navarro D, Rosso M-N, Haon M, Olivé C, Bonnin E, Lesage-Meessen L, Chevret D, Coutinho PM, Henrissat B, Berrin J-G. 2014. Fast solubilization of recalcitrant cellulosic biomass by the basidiomycete fungus *Laetisaria arvalis* involves successive secretion of oxidative and hydrolytic enzymes. Biotechnol Biofuels 7:143.

8. Hori C, Gaskell J, Igarashi K, Kersten P, Mozuch M, Samejima M, Cullen D. 2014. Temporal Alterations in the Secretome of the Selective Ligninolytic Fungus *Ceriporiopsis subvermispora* during Growth on Aspen Wood Reveal This Organism's Strategy for Degrading Lignocellulose. Appl Environ Microbiol 80:2062–2070.

9. Presley GN, Panisko E, Purvine SO, Schilling JS. 2018. Coupling secretomics with enzyme activities to compare the temporal processes of wood metabolism among white and brown rot fungi. Appl Environ Microbiol 84.

10. Zhang J, Presley GN, Hammel KE, Ryu J-S, Menke JR, Figueroa M, Hu D, Orr G, Schilling JS. 2016. Localizing gene regulation reveals a staggered wood decay mechanism for the brown rot fungus Postia placenta. Proc Natl Acad Sci 113:10968–10973.

11. Cleveland ME, Mathieu Y, Ribeaucourt D, Haon M, Mulyk P, Hein JE, Lafond M, Berrin J-G, Brumer H. 2021. A survey of substrate specificity among Auxiliary Activity Family 5 copper radical oxidases. Cell Mol Life Sci CMLS 78:8187–8208.

12. Sützl L, Laurent CVFP, Abrera AT, Schütz G, Ludwig R, Haltrich D. 2018. Multiplicity of enzymatic functions in the CAZy AA3 family. Appl Microbiol Biotechnol 102:2477–2492.

13. Bissaro B, Várnai A, Røhr ÅK, Eijsink VGH. 2018. Oxidoreductases and Reactive Oxygen Species in Conversion of Lignocellulosic Biomass. Microbiol Mol Biol Rev 82:1–51.

14. Hiner ANP, Ruiz JH, López JNR, Cánovas FG, Brisset NC, Smith AT, Arnao MB, Acosta M. 2002. Reactions of the Class II Peroxidases, Lignin Peroxidase and Arthromyces ramosus Peroxidase, with Hydrogen Peroxide. J Biol Chem 277:26879–26885.

15. Mattila H, Österman-Udd J, Mali T, Lundell T. 2022. Basidiomycota Fungi and ROS: Genomic Perspective on Key Enzymes Involved in Generation and Mitigation of Reactive Oxygen Species. Front Fungal Biol 3.

16. Castaño J, Zhang J, Zhou M, Tsai C-F, Lee JY, Nicora C, Schilling J. 2021. A Fungal Secretome Adapted for Stress Enabled a Radical Wood Decay Mechanism. mBio https://doi.org/10.1128/mBio.02040-21.

17. Lim JM, Kim G, Levine RL. 2019. Methionine in Proteins: It's Not Just for Protein Initiation Anymore. Neurochem Res 44:247–257.

18. Lourenço Dos Santos S, Petropoulos I, Friguet B. 2018. The Oxidized Protein Repair Enzymes Methionine Sulfoxide Reductases and Their Roles in Protecting against Oxidative Stress, in Ageing and in Regulating Protein Function. Antioxid Basel Switz 7:E191.

19. Rey P, Tarrago L. 2018. Physiological Roles of Plant Methionine Sulfoxide Reductases in Redox Homeostasis and Signaling. Antioxid Basel Switz 7:114.

20. Tarrago L, Kaya A, Kim H-Y, Manta B, Lee B-C, Gladyshev VN. 2022. The selenoprotein methionine sulfoxide reductase B1 (MSRB1). Free Radic Biol Med 191:228–240.

21. Erickson JR, Joiner M-LA, Guan X, Kutschke W, Yang J, Oddis C V, Bartlett RK, Lowe JS, O'Donnell SE, Aykin-Burns N, Zimmerman MC, Zimmerman K, Ham A-JL, Weiss RM, Spitz DR, Shea MA, Colbran RJ, Mohler PJ, Anderson ME. 2008. A Dynamic Pathway for Calcium-Independent Activation of CaMKII by Methionine Oxidation. Cell 133:462–474.

22. Hou L, Kang I, Marchant RE, Zagorski MG. 2002. Methionine 35 Oxidation Reduces Fibril Assembly of the Amyloid Aβ-(1–42) Peptide of Alzheimer's Disease. J Biol Chem 277:40173–40176.

23. Levine RL, Mosoni L, Berlett BS, Stadtman ER. 1996. Methionine residues as endogenous antioxidants in proteins. Proc Natl Acad Sci U S A 93:15036–15040.

24. Hage H, Rosso M-N, Tarrago L. 2021. Distribution of methionine sulfoxide reductases in fungi and conservation of the free-methionine-R-sulfoxide reductase in multicellular eukaryotes. Free Radic Biol Med 169:187–215.

25. Kachurin AM, Golubev AM, Geisow MM, Veselkina OS, Isaeva-Ivanova LS, Neustroev KN. 1995. Role of methionine in the active site of α-galactosidase from *Trichoderma reesei*. Biochem J 308:955–964.

26. Miyauchi S, Hage H, Drula E, Lesage-Meessen L, Berrin JG, Navarro D, Favel A, Chaduli D, Grisel S, Haon M, Piumi F, Levasseur A, Lomascolo A, Ahrendt S, Barry K, LaButti KM, Chevret D, Daum C, Mariette J, Klopp C, Cullen D, de Vries RP, Gathman AC, Hainaut M, Henrissat B, Hildén KS, Kües U, Lilly W, Lipzen A, Mäkelä MR, Martinez AT, Morel-Rouhier M, Morin E, Pangilinan J, Ram AFJ, Wösten HAB, Ruiz-Dueñas FJ, Riley R, Record E, Grigoriev I V., Rosso MN. 2020. Conserved white-rot enzymatic mechanism for wood decay in the Basidiomycota genus Pycnoporus. DNA Res Int J Rapid Publ Rep Genes Genomes 27:1–14.

27. Bettinger JQ, Simon M, Korotkov A, Welle KA, Hryhorenko JR, Seluanov A, Gorbunova V, Ghaemmaghami S. 2022. Accurate Proteomewide Measurement of Methionine Oxidation in Aging Mouse Brains. J Proteome Res 21:1495–1509.

28. Bettinger JQ, Welle KA, Hryhorenko JR, Ghaemmaghami S. 2020. Quantitative Analysis of in Vivo Methionine Oxidation of the Human Proteome. J Proteome Res 19:624–633.

29. Liu H, Ponniah G, Neill A, Patel R, Andrien B. 2013. Accurate determination of protein methionine oxidation by stable isotope labeling and LC-MS analysis. Anal Chem 85:11705–11709.

30. Shipman JT, Go EP, Desaire H. 2018. Method for Quantifying Oxidized Methionines and Application to HIV-1 Env. J Am Soc Mass Spectrom 29:2041–2047.

31. Hartmann EM, Allain F, Gaillard J-C, Pible O, Armengaud J. 2014. Taking the shortcut for high-throughput shotgun proteomic analysis of bacteria. Methods Mol Biol Clifton NJ 1197:275–285.

32. Lozano C, Grenga L, Gallais F, Miotello G, Bellanger L, Armengaud J. 2023. Mass spectrometry detection of monkeypox virus: Comprehensive coverage for ranking the most responsive peptide markers. Proteomics 23:e2200253.

33. Paoletti AC, Parmely TJ, Tomomori-Sato C, Sato S, Zhu D, Conaway RC, Conaway JW, Florens L, Washburn MP. 2006. Quantitative proteomic analysis of distinct mammalian Mediator complexes using normalized spectral abundance factors. Proc Natl Acad Sci 103:18928–18933.

34. Perez-Riverol Y, Bai J, Bandla C, García-Seisdedos D, Hewapathirana S, Kamatchinathan S, Kundu DJ, Prakash A, Frericks-Zipper A, Eisenacher M, Walzer M, Wang S, Brazma A, Vizcaíno JA. 2021. The PRIDE database resources in 2022: a hub for mass spectrometry-based proteomics evidences. Nucleic Acids Res 50:D543–D552.

35. Arfi Y, Chevret D, Henrissat B, Berrin J-G, Levasseur A, Record E. 2013. Characterization of salt-adapted secreted lignocellulolytic enzymes from the mangrove fungus *Pestalotiopsis* sp. Nat Commun 4:1810.

36. Arntzen MØ, Bengtsson O, Várnai A, Delogu F, Mathiesen G, Eijsink VGH. 2020. Quantitative comparison of the biomass-degrading enzyme repertoires of five filamentous fungi. Sci Rep 10:20267.

37. Couturier M, Navarro D, Chevret D, Henrissat B, Piumi F, Ruiz-Dueñas FJ, Martinez AT, Grigoriev IV, Riley R, Lipzen A, Berrin J-G, Master ER, Rosso M-N. 2015. Enhanced degradation of softwood versus hardwood by the white-rot fungus *Pycnoporus coccineus*. Biotechnol Biofuels 8:216.

572 38. Couturier M, Navarro D, Olivé C, Chevret D, Haon M, Favel A, Lesage-Meessen L, Henrissat B,
573 Coutinho PM, Berrin J-G. 2012. Post-genomic analyses of fungal lignocellulosic biomass
574 degradation reveal the unexpected potential of the plant pathogen *Ustilago maydis*. BMC
575 Genomics 13:57.

576 39. Daou M, Farfan Soto C, Majira A, Cézard L, Cottyn B, Pion F, Navarro D, Oliveira Correia L, Drula
577 E, Record E, Raouche S, Baumberger S, Faulds CB. 2021. Fungal Treatment for the Valorization
578 of Technical Soda Lignin. J Fungi Basel Switz 7:39.

579 40. Filiatrault-Chastel C, Navarro D, Haon M, Grisel S, Herpoël-Gimbert I, Chevret D, Fanuel M,
580 Henrissat B, Heiss-Blanquet S, Margeot A, Berrin J-G. 2019. AA16, a new lytic polysaccharide
581 monooxygenase family identified in fungal secretomes. Biotechnol Biofuels 12:55.

582 41. Levasseur A, Lomascolo A, Chabrol O, Ruiz-Dueñas FJ, Boukhris-Uzan E, Piumi F, Kües U, Ram
583 AFJ, Murat C, Haon M, Benoit I, Arfi Y, Chevret D, Drula E, Kwon MJ, Gouret P, Lesage-Meessen
584 L, Lombard V, Mariette J, Noirot C, Park J, Patyshakuliyeva A, Sigoillot JC, Wiebenga A, Wösten
585 HAB, Martin F, Coutinho PM, de Vries RP, Martínez AT, Klopp C, Pontarotti P, Henrissat B,
586 Record E. 2014. The genome of the white-rot fungus *Pycnoporus cinnabarinus*: a basidiomycete
587 model with a versatile arsenal for lignocellulosic biomass breakdown. BMC Genomics 15:486.

588 42. Miyauchi S, Hage H, Drula E, Lesage-Meessen L, Berrin J-G, Navarro D, Favel A, Chaduli D, Grisel
589 S, Haon M, Piumi F, Levasseur A, Lomascolo A, Ahrendt S, Barry K, LaButti KM, Chevret D, Daum
590 C, Mariette J, Klopp C, Cullen D, de Vries RP, Gathman AC, Hainaut M, Henrissat B, Hildén KS,
591 Kües U, Lilly W, Lipzen A, Mäkelä MR, Martinez AT, Morel-Rouhier M, Morin E, Pangilinan J,
592 Ram AFJ, Wösten HAB, Ruiz-Dueñas FJ, Riley R, Record E, Grigoriev IV, Rosso M-N. 2020.
593 Conserved white-rot enzymatic mechanism for wood decay in the Basidiomycota genus
594 Pycnoporus. DNA Res Int J Rapid Publ Rep Genes Genomes 27.

595 43. Miyauchi S, Rancon A, Drula E, Hage H, Chaduli D, Favel A, Grisel S, Henrissat B, Herpoël-
596 Gimbert I, Ruiz-Dueñas FJ, Chevret D, Hainaut M, Lin J, Wang M, Pangilinan J, Lipzen A, Lesage-
597 Meessen L, Navarro D, Riley R, Grigoriev IV, Zhou S, Raouche S, Rosso M-N. 2018. Integrative
598 visual omics of the white-rot fungus *Polyporus brumalis* exposes the biotechnological potential
599 of its oxidative enzymes for delignifying raw plant biomass. Biotechnol Biofuels 11:201.

600 44. Miyauchi S, Navarro D, Grisel S, Chevret D, Berrin J-G, Rosso M-N. 2017. The integrative omics
601 of white-rot fungus *Pycnoporus coccineus* reveals co-regulated CAZymes for orchestrated
602 lignocellulose breakdown. PLoS ONE 12:e0175528.

603 45. Miyauchi S, Navarro D, Grigoriev IV, Lipzen A, Riley R, Chevret D, Grisel S, Berrin J-G, Henrissat
604 B, Rosso M-N. 2016. Visual Comparative Omics of Fungi for Plant Biomass Deconstruction. Front
605 Microbiol 7.

606 46. Paës G, Navarro D, Benoit Y, Blanquet S, Chabbert B, Chaussepied B, Coutinho PM, Durand S,
607 Grigoriev IV, Haon M, Heux L, Launay C, Margeot A, Nishiyama Y, Raouche S, Rosso M-N, Bonnin
608 E, Berrin J-G. 2019. Tracking of enzymatic biomass deconstruction by fungal secretomes
609 highlights markers of lignocellulose recalcitrance. Biotechnol Biofuels 12:76.

610 47. Poidevin L, Berrin J-G, Bennati-Granier C, Levasseur A, Herpoël-Gimbert I, Chevret D, Coutinho
611 PM, Henrissat B, Heiss-Blanquet S, Record E. 2014. Comparative analyses of Podospora
612 anserina secretomes reveal a large array of lignocellulose-active enzymes. Appl Microbiol
613 Biotechnol 98:7457–7469.

614 48. Reyre J-L, Grisel S, Haon M, Navarro D, Ropartz D, Le Gall S, Record E, Sciara G, Tranquet O,
615 Berrin J-G, Bissaro B. 2022. The Maize Pathogen *Ustilago maydis* Secretes Glycoside Hydrolases
616 and Carbohydrate Oxidases Directed toward Components of the Fungal Cell Wall. Appl Environ
617 Microbiol 88:e0158122.

49. Ribeaucourt D, Saker S, Navarro D, Bissaro B, Drula E, Correia LO, Haon M, Grisel S, Lapalu N, Henrissat B, O'Connell RJ, Lambert F, Lafond M, Berrin J-G. 2021. Identification of Copper-Containing Oxidoreductases in the Secretomes of Three *Colletotrichum* Species with a Focus on Copper Radical Oxidases for the Biocatalytic Production of Fatty Aldehydes. Appl Environ Microbiol 87:e0152621.

50. Meinken J, Asch DK, Neizer-Ashun KA, Chang G-H, R.Cooper JR C, Min XJ. 2014. FunSecKB2: a fungal protein subcellular location knowledgebase. Comput Mol Biol https://doi.org/10.5376/CMB.2014.04.0007.

51. Meinken J, Walker G, Cooper CR, Min XJ. 2015. MetazSecKB: the human and animal secretome and subcellular proteome knowledgebase. Database 2015:1–14.

52. Uhlén M, Fagerberg L, Hallström BM, Lindskog C, Oksvold P, Mardinoglu A, Sivertsson Å, Kampf C, Sjöstedt E, Asplund A, Olsson IM, Edlund K, Lundberg E, Navani S, Szigyarto CAK, Odeberg J, Djureinovic D, Takanen JO, Hober S, Alm T, Edqvist PH, Berling H, Tegel H, Mulder J, Rockberg J, Nilsson P, Schwenk JM, Hamsten M, Von Feilitzen K, Forsberg M, Persson L, Johansson F, Zwahlen M, Von Heijne G, Nielsen J, Pontén F. 2015. Tissue-based map of the human proteome. Science 347.

53. Uhlén M, Karlsson MJ, Hober A, Svensson AS, Scheffel J, Kotol D, Zhong W, Tebani A, Strandberg L, Edfors F, Sjöstedt E, Mulder J, Mardinoglu A, Berling A, Ekblad S, Dannemeyer M, Kanje S, Rockberg J, Lundqvist M, Malm M, Volk AL, Nilsson P, Månberg A, Dodig-Crnkovic T, Pin E, Zwahlen M, Oksvold P, von Feilitzen K, Häussler RS, Hong MG, Lindskog C, Ponten F, Katona B, Vuu J, Lindström E, Nielsen J, Robinson J, Ayoglu B, Mahdessian D, Sullivan D, Thul P, Danielsson F, Stadler C, Lundberg E, Bergström G, Gummesson A, Voldborg BG, Tegel H, Hober S, Forsström B, Schwenk JM, Fagerberg L, Sivertsson Å. 2019. The human secretome. Sci Signal 12.

54. Lum G, Meinken J, Orr J, Frazier S, Min XJ. 2014. PlantSecKB: the Plant Secretome and Subcellular Proteome KnowledgeBase. Comput Mol Biol 4.

55. Hooper CM, Castleden IR, Tanz SK, Aryamanesh N, Millar AH. 2017. SUBA4: the interactive data analysis centre for Arabidopsis subcellular protein locations. Nucleic Acids Res 45:D1064–D1074.

56. Zhao Z, Liu H, Wang C, Xu JR. 2014. Correction to Comparative analysis of fungal genomes reveals different plant cell wall degrading capacity in fungi [BMC Genomics 14(2013) 274]. BMC Genomics 15:1–15.

57. Miyauchi S, Kiss E, Kuo A, Drula E, Kohler A, Sánchez-García M, Morin E, Andreopoulos B, Barry KW, Bonito G, Buée M, Carver A, Chen C, Cichocki N, Clum A, Culley D, Crous PW, Fauchery L, Girlanda M, Hayes RD, Kéri Z, LaButti K, Lipzen A, Lombard V, Magnuson J, Maillard F, Murat C, Nolan M, Ohm RA, Pangilinan J, Pereira M de F, Perotto S, Peter M, Pfister S, Riley R, Sitrit Y, Stielow JB, Szöllősi G, Žifčáková L, Štursová M, Spatafora JW, Tedersoo L, Vaario L-M, Yamada A, Yan M, Wang P, Xu J, Bruns T, Baldrian P, Vilgalys R, Dunand C, Henrissat B, Grigoriev I V., Hibbett D, Nagy LG, Martin FM. 2020. Large-scale genome sequencing of mycorrhizal fungi provides insights into the early evolution of symbiotic traits. Nat Commun 11:5125.

58. Camacho C, Coulouris G, Avagyan V, Ma N, Papadopoulos J, Bealer K, Madden TL. 2009. BLAST+: architecture and applications. BMC Bioinformatics 10:421.

59. Katoh K, Rozewicki J, Yamada KD. 2019. MAFFT online service: multiple sequence alignment, interactive sequence choice and visualization. Brief Bioinform 20:1160–1166.

60. UniProtKB/Swiss-Prot Release 2023_04 statistics. https://web.expasy.org/docs/relnotes/relstat.html. Retrieved 14 September 2023.

61. Hawkins CL, Davies MJ. 2019. Detection, identification, and quantification of oxidative protein modifications. J Biol Chem 294:19683–19708.

62. Varadi M, Anyango S, Deshpande M, Nair S, Natassia C, Yordanova G, Yuan D, Stroe O, Wood G, Laydon A, Žídek A, Green T, Tunyasuvunakool K, Petersen S, Jumper J, Clancy E, Green R, Vora A, Lutfi M, Figurnov M, Cowie A, Hobbs N, Kohli P, Kleywegt G, Birney E, Hassabis D, Velankar S. 2022. AlphaFold Protein Structure Database: massively expanding the structural coverage of protein-sequence space with high-accuracy models. Nucleic Acids Res 50:D439–D444.

63. Ezraty B, Grimaud R, El Hassouni M, Moinier D, Barras F. 2004. Methionine sulfoxide reductases protect Ffh from oxidative damages in *Escherichia coli*. EMBO J 23:1868–1877.

64. Laugier E, Tarrago L, Vieira Dos Santos C, Eymery F, Havaux M, Rey P. 2010. *Arabidopsis thaliana* plastidial methionine sulfoxide reductases B, MSRBs, account for most leaf peptide MSR activity and are essential for growth under environmental constraints through a role in the preservation of photosystem antennae. Plant J Cell Mol Biol 61:271–282.

65. Rouyère C, Serrano T, Frémont S, Echard A. 2022. Oxidation and reduction of actin: Origin, impact in vitro and functional consequences in vivo. Eur J Cell Biol 101:151249.

66. Bender A, Hajieva P, Moosmann B. 2008. Adaptive antioxidant methionine accumulation in respiratory chain complexes explains the use of a deviant genetic code in mitochondria. Proc Natl Acad Sci U S A 105:16496–16501.

67. Melnyk RA, Youngblut MD, Clark IC, Carlson HK, Wetmore KM, Price MN, Iavarone AT, Deutschbauer AM, Arkin AP, Coates JD. 2015. Novel mechanism for scavenging of hypochlorite involving a periplasmic methionine-rich Peptide and methionine sulfoxide reductase. mBio 6:e00233-00215.

685 68. Luo S, Levine RL. 2009. Methionine in proteins defends against oxidative stress. FASEB J Off
686 Publ Fed Am Soc Exp Biol 23:464–472.

687 69. Castaño JD, Zhou M, Jonathan Schilling. 2021. Towards an Understanding of Oxidative Damage
688 in an α-L-Arabinofuranosidase of *Trichoderma reesei*: a Molecular Dynamics Approach. Appl
689 Biochem Biotechnol 193:3287–3300.

690 70. Peciulyte A, Samuelsson L, Olsson L, McFarland KC, Frickmann J, Østergård L, Halvorsen R, Scott
691 BR, Johansen KS. 2018. Redox processes acidify and decarboxylate steam-pretreated
692 lignocellulosic biomass and are modulated by LPMO and catalase. Biotechnol Biofuels 11:165.

693 71. Scott BR, Huang HZ, Frickman J, Halvorsen R, Johansen KS. 2016. Catalase improves
694 saccharification of lignocellulose by reducing lytic polysaccharide monooxygenase-associated
695 enzyme inactivation. Biotechnol Lett 38:425–434.

696 72. Kwon S-I, Anderson AJ. 2001. Catalase Activities of *Phanerochaete chrysosporium* Are Not
697 Coordinately Produced with Ligninolytic Metabolism: Catalases from a White-Rot Fungus. Curr
698 Microbiol 42:8–11.

699 73. Hansberg W, Salas-Lizana R, Domínguez L. 2012. Fungal catalases: function, phylogenetic origin
700 and structure. Arch Biochem Biophys 525:170–180.

701 74. Tarrago L, Grosse S, Siponen MI, Lemaire D, Alonso B, Miotello G, Armengaud J, Arnoux P,
702 Pignol D, Sabaty M. 2018. *Rhodobacter sphaeroides* methionine sulfoxide reductase P reduces
703 R- and S-diastereomers of methionine sulfoxide from a broad-spectrum of protein substrates.
704 Biochem J 475:3779–3795.

705